Spectral function analysis on the Holstein polaron problem

Extraction of the self-energy and coupling strength, and their implications for angle resolved photoemission spectroscopy

by

Christian Neil Veenstra

B.Sc., McMaster University, 2005

A THESIS SUBMITTED IN PARTIAL FULFILMENT OF
THE REQUIREMENTS FOR THE DEGREE OF

Master of Science

in

The Faculty of Graduate Studies

(Physics)

October 2007

Abstract

This thesis first reviews and examines the Angle Resolved Photoemission Spectroscopy (ARPES) experiment. It is shown that the spectral density function, familiar from the Green's function method of studying correlated systems, can be directly measured. A model spectral function with a non-trivial self-energy is then used to test an improvement to a recently arrived method[15, 17] to analyze ARPES data.

This new method relies on self-consistency between the real and imaginary parts of the self-energy (as measured through the Kramers-Kronig transform) to overcome the requirement of knowing the bare electronic structure. Through this, the method extracts both the complex self-energy and the bare electronic structure from the spectral function.

The method described here is an improvement on this idea as previously implemented in that a strict form for the bare band dispersion (previously considered linear or quadratic) is never assumed. Although the method here utilized a polynomial of arbitrary degree, it could be trivially expanded to use any other functional form so long as both the value and first derivative are known analytically as a function of the fitting parameters.

Using Mona Berciu's first order momentum average (MA) approximation[2] as implemented by Glen Goodvin[8] the spectral function as well as momentum independent self-energy were calculated for the Holstein polaron for a wide range of parameters. It was found that self-consistent spectral function analysis was highly successful at extracting the self energy and bare electronic dispersion from the spectral function over a consistent subset of these parameters.

For studies outside this range of parameters the more traditional ARPES analysis method of measuring renormalization is also examined.

Table of Contents

List of Figures

List of Abbreviations

ARPES Angle Resolved PhotoEmission Spectroscopy (sometimes Angle Resolved PhotoElectron Spectroscopy)

dHvA - de Haas-van Alphen

DFT - Density Funcional Theorem

EDC - Energy Distribution Curve

FFT - Fast Fourier Transform

FWHM - Full Width Half Maximum

HWHM - Half Width Half Maximum

KK - Kramers-Kronig

LDA - Local-Density Approximation

MA - Momentum Average (approximation)

MDC - Momentum Distribution Curve

PES - PhotoElectron Spectroscopy (sometimes PhotoEmission Spectroscopy)

QMC - Quantum Monte Carlo

SCBA - Self-Consistent Born Approximation

SLS - Swiss Light Source, Paul Scherrer Institut, Switzerland

SRC - Synchrotron Radiation Center, Wisconsin, USA

SXPS - Soft Xray PhotoEmission Spectroscopy

UBC - University of British Columbia

UHV - Ultra High Vacuum

UPS - Ultraviolet PhotoEmission Spectroscopy

UV - Ultra Violet

XPS - Xray PhotoEmission Spectroscopy

Acknowledgements

I would like to thank my supervisor Dr. Andrea Damascelli, as well as my de facto secondary supervisor Dr. Nicholas Ingle, who have been the source of my experimental physics education, and have taught me so much in addition to just how to *do* ARPES. Andrea's (sometimes forceful by necessity) guidance and Nik's lessons on human phycology and interactions have made my continued existence as a grad student possible.

I must certainly thank Glen Goodvin and Dr. Mona Berciu, who provided me with the source code used to implement their Momentum Averaging method. Having access to a physically satisfying model which can be quickly calculated over a wide range of parameters played a key role in the development of this thesis. Discussions with Mona also played a key role in my understanding of the polaron problem, and I look forward to future discussions.

Additionally I would like to thank my brothers-in-arms - the other graduate students in the quantum materials lab Jeff Mottershead, Ryan Wicks, Jonathan Rosen and Suman Hossian, as well as post docs Thomas Roth and David Fournier, and our current visiting professor Giancarlo Panaccione. Bouncing ideas off smart people is an excellent (and perhaps the only?) way to properly formulate them to yourself, and the other members of our group have always stepped up to the plate.

Numerous friends and housemates also kept me physically alive during the writing of this thesis, whether by intentionally feeding me or forgiving me when I ate food they'd mistakenly left somewhere I could find it. Sandra, in particular, proved herself outstanding once again and even proofread parts of this thesis - despite the fact she is a biology student, racking up an exceedingly high number of beers owed for having being subjected to so many equations. Line, my girlfriend, also had the good sense to support me by returning home to Denmark, thus giving me ample time to escape to the office for the many late nights required to finally finish this thing.

Finally, I thank the Natural Science and Engineering Research Council of Canada for funding during these first two years of graduate study.

Chapter 1

Introduction

1.1 Correlated systems

In the constant drive to explain the world around us, physics has reached a new hurdle. The understanding of amazing properties like unconventional and high-temperature superconductivity, colossal magnetoresistance, and Mott-Hubbard insulations test our current theoretical and experimental limits.

In the so-called *golden years* of physics, the first half of the twentieth century, there was a staggering re-organization in our understanding of the world around us. The emerging pillars of modern physics, quantum theory and relativity, were fantastic - even irrational - compared to the 'laws' as understood by humankind not even a century before. Tested by experiment, these are the rules by which we now play.

So what, then, can this next hurdle be? The laws describing the world around us, at least at the energy and distance scale of these new phenomena, have been well understood for over half a century. However, as we have now discovered, it requires more than a mere knowledge of the rules to play the game.

In *correlated systems* we see the results of the interplay between particles in a many body problem. Although even an undergraduate level physics education includes the fundamental rules of a quantum mechanical world, correlations between particles can cause strange behaviour as soon as the number of interacting members is greater than two. Sometimes these systems can be explained by the independent particle picture with correlations added as a perturbation. Sometimes not. In systems with upwards of 10^{24} members, it should be no surprise that the possibilities are seemingly endless.

The description of these systems has seen the introduction of a new cast of characters. *Quasi-particles* as well as *collective modes* such as *phonons* and *magnons* name just a few of the roles, often played by actors from the entire system. These new descriptions have breathed life into these excitations, which are often treated as if they were themselves actual particles

with their own interactions and correlations.

This new age in condensed matter physics will be in the description not of the fundamental laws, but in the discovering of new ways to move within them. As has been said of many games - it may take but a moment to learn the rules, but a lifetime to master the possibilities.

As both a motivation and a crucible for these discoveries we have, as always, experiment.

1.2 Angle resolved photoemission

Beginning as an unexplained phenomena in 1887 with Hertz's photoelectric effect [10] and Einstein's Nobel-prize winning explanation [7], photoemission has now become an indispensable tool in the discovery of new quantum phenomena.

Angle-Resolved Photoemission Spectroscopy (ARPES) is, simply put, the flux of photoemitted electrons measured as a function of both angle and energy. This chapter will strive to clarify the basic physical setup of a modern ARPES system, the deeper question of what is actually measured with the technique, and perhaps most importantly - why we might actually care to use it to study correlated systems.

In short, I hope it to be the introduction to ARPES, correlated systems and the Green's function I wish I had had access to when I first set foot in the ARPES lab here at UBC - more succinct and focused than a stack of textbooks, yet with more detail than could be expected from a paper published for those already expert in the field.

1.2.1 Photoemission

We start with (energy-resolved) PhotoEmission Spectroscopy (PES), often called PhotoElectron Spectroscopy. Although more refined, the principles of PES today are the same as over a century ago. A monochromatic light source with known photon energy, $h\nu$, is used to excite electrons in a sample held in vacuum. If the new total energy of the electrons is sufficient they may leave the sample, a process known as *photoemission*. Once in vacuum the kinetic energy, E_k, of these *photoelectrons* may be measured. A consistent amount of energy, the so-called *workfunction*, Φ, is required to overcome the surface and escape the sample. With knowledge of this workfunction, the photon energy, $h\nu$, and the kinetic energy one then has direct access to the binding energy, E_b, of the electrons in the sample through energy

conservation:

$$E_k = h\nu - \Phi_{\text{sample}} - E_b \tag{1.1}$$

A diagrammatic representation of the energetics of this process compared to actual photoemission data is presented in Figure 1.1 and Figure 1.2.

The energy resolution and accessible range vary with photon energy and detector. In practice photon energies in the ranges 0-100eV (Ultraviolet Photoemission Spectroscopy - UPS), 100-1000eV (Soft X-ray Photoemission Spectroscopy - SXPS), and >1000eV (X-ray Photoemission Spectroscopy - XPS) are used to study a variety of binding energies. The photon energy must be chosen carefully depending on what the experimentalist wishes to study. For studies near the *Fermi energy* low energy photoemission usually offers better resolution, typically done using UPS, while to study core-level properties XPS is required in order to have enough energy to liberate the electrons in the first place.

The photon energy also has an affect on the depth at which information is collected. The *universal curve* for electron mean free path, Figure 1.3, has a strong dependance on energy. This is directly related to the escape depth of photoemitted electrons. Since typical lattice spacings for many of the materials studied are on the order of Angstroms the result is that, depending on photon energy, photoemission can be either surface sensitive or highly surface sensitive. In the field of photoemission, data collected from a depth of only 10 monolayers would be considered a bulk measurement.

1.2.2 The ARPES experiment

An ARPES setup involves a monochromatic light source incident on a sample in ultra-high vacuum (UHV). The source is typically a synchrotron, gas discharge lamp or more recently, a UV laser. A subset of the photoemitted electrons from this sample are collected by an analyzer capable of resolving both energy and momentum over a specified acceptance window and a two dimensional spectrum of intensity vs. angle and energy is produced. Figure 1.4 depicts a typical ARPES geometry, while Figure 1.5 shows typical ARPES data.

The goal in examining this data is to relate the measured quantities to the original electronic properties of the sample.

The momentum of the electron in vacuum is completely determined through the kinematic relation:

$$|\vec{p}| = \sqrt{2m_e E_k} \tag{1.2}$$

Figure 1.1: Relation between the electronic structure of a solid and its photoemission spectrum produced by photons of energy $h\nu$. From Ref [12]. As every photon provides the same amount of energy, the spectrum of kinetic energy resolved in experiment will directly reflect the original energy structure in the sample. The binding energy, E_b, is defined as the energy from the Fermi energy, E_f, the highest occupied energy in the sample's electronic structure. E_f is easily identified in experiment as the upper bound on observed kinetic energy and is therefore a convenient 'zero' from which to measure.
In this diagram we can identify *core level* electronic states, those bound to a single atom in the sample and highly localized in energy, as well as a *valence band* originating from the overlapping and hybridized valence orbitals in the sample lattice which occupies a finite but continuous energy range.

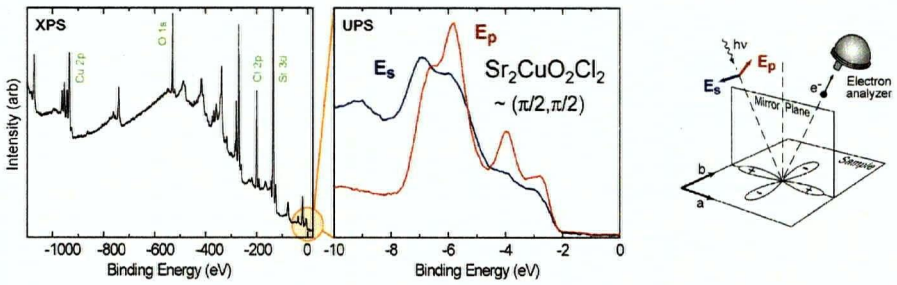

Figure 1.2: Photoemission from $Sr_2CuO_2Cl_2$ over a wide energy rage using two different techniques. At left is XPS, with selected core electron orbitals labeled. In center is UPS data on the same material to demonstrate and compare the energy range possible with each technique. In this particular experiment, the polarization of the photons was varied as shown at right. The striking difference in intensity based solely on photon polarization comes from the so-called matrix element effects in Equation 1.9. Note that the rise in intensity at $E_{\text{binding}} = -2\text{eV}$ is not due to the Fermi energy, but appearance of oxygen valence bands. By definition, the binding energy is zero at E_{Fermi}. In this material, an insulator, the Fermi energy is not visible and would need to be determined from a reference sample. The Fermi energy is clearly visible on the bottom half of Figure 1.5. Data taken by our group, with our ARPES chamber at UBC.

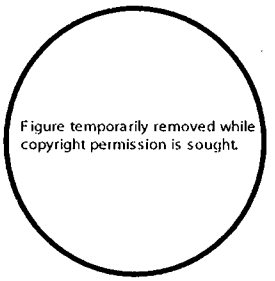

Figure 1.3: The so-called *universal curve* of inelastic mean free path for electrons in a variety of materials. This is directly related to the escape depth from which we can expect electrons to photoemit from these materials. Although there is a spread in the data reflecting the large variety of materials sampled, there is a clear trend which gives rise to its name. From Ref [23].

Where the direction of momentum can be determined from the measured photoemission angle. For the photon energies used in ARPES, the photon momentum is negligible on the momentum scale of the electron. Since components of electron momentum in plane with the sample surface must be conserved, due to symmetry, the measured in-plane momentum is equivalent to the original momentum in the sample. Although the momentum perpendicular to the sample surface is not conserved, this potential problem can be avoided by choosing quasi 2d systems with little dispersion in the out-of-plane direction.

Finally, good electrical conduction between all elements of the system ensures that the Fermi levels, E_f of analyzer and sample are aligned, thus the measured photon energy is given by:

$$E_{\text{in analyzer}} + \Phi_{\text{analyzer}} = E_{\text{in vacuo}} + \Phi_{\text{sample}} \tag{1.3}$$

With Eqn 1.1 and $E_{\text{kinetic}} = E_{\text{in vacuo}}$ this becomes:

$$E_{\text{measured}} = E_{\text{in analyzer}} = h\nu - \Phi_{\text{analyzer}} - E_b \tag{1.4}$$

Note that, with good conduction between sample and analyzer, the workfunction of the sample is not measured by ARPES. Only the workfunction of

Figure 1.4: Experimental setup of an ARPES Experiment. From Ref [4]. Photons incident on the sample cause electrons to be emitted, which are then collected by the analyzer. The electrostatic lens performs two functions. It employs Fourier optics, which map angle to position, in order to resolve the angle of accepted electrons. As well it employs an acceleration/retardation potential to bring the electrons to a selected 'pass energy' which will allow them to pass around the hemispherical capacitor. Thus, by the time the electrons reach the detector the angle of electrons, θ_x, will be resolved in the direction tangent to the hemisphere, while the energy, E_k, will be resolved parallel to the radius of the hemisphere.

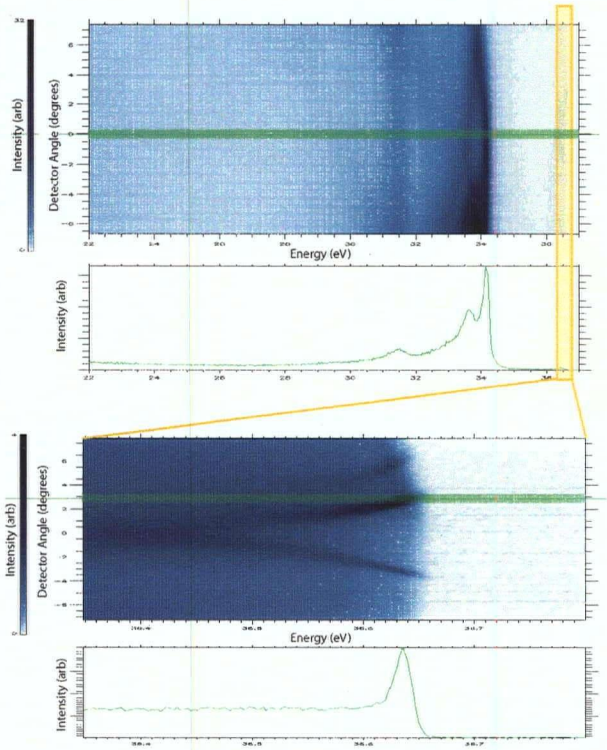

Figure 1.5: ARPES on S_2RuO_4, taken at the Synchrotron Radiation Center (SRC). The intensity is a 2 dimensional function of angle and energy, with an energy slice shown underneath to allow a comparison of scale. The energy scale in this case is the kinetic energy of the electron, and has not yet been adjusted to binding energy relative to the Fermi surface. The upper window shows a large energy range, where the oxygen bands (centered around 34eV) can be clearly seen (as in Figure 1.2). In the lower panel is a zoomed in picture near the Fermi energy, where highly momentum (angle) dependent electronic structure can be seen.

the analyzer itself appears, provided that the photon has enough energy to liberate the electron in the first place. This allows one to measure E_f from a polycrystalline 'good' metal reference sample (gold, for example), and use that reference to determine E_b on the sample of interest. This is important, as both Φ_{analyzer} and $h\nu$ are often not know precisely. In this manner the binding energy of the electrons is accessible.

With these two relationships, Equation 1.2 and 1.4, ARPES thus measures both the original binding energy and in-plane momentum of all photoemitted electrons collected.

1.3 What we see with ARPES

This section will seek to answer two of the goals eluded to above. Namely, what we actually measure with ARPES and why we would use it to study correlated systems. Here the *spectral function* will be introduced and through it a strong connection made to the *Green's function* method of studying correlated systems.

1.3.1 The photoemission process

We saw in § 1.2.2 that ARPES should measure both the binding energy and the in-plane momentum of the electron photoemitted. Let us now look with more care at what we actually measure with photoemission, and how it relates to the structure of the underlying system. An important approximation often made is the so-called *sudden approximation* [4, 12], which is to say we assume that the escaping photon does not interact with the remaining system (for conditions see [9]).

Under this sudden approximation, we may start by using Fermi's Golden Rule [6] to describe the interaction of the electron with the photon as a transition between the original in-sample electronic state to the free particle continuum in vacuum, with the photon as the perturbation. The transition probability, $\omega_{f\to i}$, to final state Ψ_f^N from initial state Ψ_i^N with an interaction perturbation from the photon, H_{int}, is then given by [12]:

$$\omega_{f\to i} = \frac{2\pi}{\hbar} \left|\left\langle \Psi_f^N \right| H_{\text{int}} \left|\Psi_i^N\right\rangle\right|^2 \delta\left(E_f^N - E_i^N - h\nu\right) \tag{1.5}$$

$$H_{\text{int}} = \frac{e}{2mc}\left(\overrightarrow{A}\cdot\mathbf{p} + \mathbf{p}\cdot\overrightarrow{A}\right) - e\phi + \frac{e^2}{2mc^2}\overrightarrow{A}\cdot\overrightarrow{A} \tag{1.6}$$

Where $\mathbf{p}$ is the momentum operator and $\overrightarrow{A}$ and ϕ the vector and scalar

potentials. Here we may simplify Equation 1.6 by using the gauge $\phi = 0$, the commutation relation $[\mathbf{p}, \overrightarrow{A}] = -i\hbar\nabla \cdot \overrightarrow{A}$, under the dipole approximation $\nabla \cdot \overrightarrow{A} = 0$ and neglecting the two photon process, $\overrightarrow{A} \cdot \overrightarrow{A}$:

$$\omega_{f\to i} = \frac{2\pi e}{\hbar mc} \left| \left\langle \Psi_f^N \right| \overrightarrow{A} \cdot \mathbf{p} \left| \Psi_i^N \right\rangle \right|^2 \delta \left(E_f^N - E_i^N - h\nu \right) \tag{1.7}$$

Now we expand the initial and final states into their components via the antisymmetric combinations operator $\mathcal{A}[\ ]$ into $\Psi_f^N = \mathcal{A}\left[\phi_f^k \psi_f^{N-1}\right]$ and $\Psi_i^N = \mathcal{A}\left[\phi_i^k \psi_i^{N-1}\right]$, where ϕ_f^k is the photoemitted electron, ψ_f^{N-1} is the excited state of the $N-1$ particle Hamiltonian left behind, ϕ_i^k is the state from which the electron will be photoemitted and ψ_i^{N-1} represents the remainder of the system. This allows us to re-write Equation 1.7 as:

$$\omega_{f\to i} = \frac{2\pi e}{\hbar mc} \left| \left\langle \phi_f^k \right| \overrightarrow{A} \cdot \mathbf{p} \left| \phi_i^k \right\rangle \right|^2 \left| \left\langle \psi_f^{N-1} \middle| \psi_i^{N-1} \right\rangle \right|^2 \delta \left(E_f^{N-1} + E_k^{e^-} - E_i^N - h\nu \right) \tag{1.8}$$

In a non-interacting picture ψ_f^{N-1} and ψ_i^{N-1} would be identical as the electronic structure would be unaffected by the removal of an electron and only the filling would change. In this instance Equation 1.8 would become a delta-function following the electron bandstructure, modulated in intensity by the so-called *matrix element effects*, $\left| \left\langle \phi_f^k \right| \overrightarrow{A} \cdot \mathbf{p} \left| \phi_i^k \right\rangle \right|^2$, a measure of the coupling between electron and photon, which depends on experimental geometry and polarization.

A more realistic approach would express ψ_f^{N-1} as a sum over all excited states of the $N-1$ Hamiltonian, ψ_n^{N-1} with energy E_n^{N-1}. ψ_i^{N-1} could be expressed as the original state acted on by the appropriate annihilation operator to remove the state ϕ_i^k, such that $\psi_i^{N-1} = c_k \psi_i^N$. This approach yields:

$$\omega_{f\to i} = \frac{2\pi e}{\hbar mc} \left| \left\langle \phi_f^k \right| \overrightarrow{A} \cdot \mathbf{p} \left| \phi_i^k \right\rangle \right|^2 \sum_n \left| \left\langle \psi_n^{N-1} \right| c_k \left| \psi_i^N \right\rangle \right|^2 \delta \left(E_n^{N-1} + E_k^{e^-} - E_i^N - h\nu \right) \tag{1.9}$$

In Equation 1.9 we recognize both the aforementioned matrix element effects and terms reflecting the one-electron removal probability. This removal

probability, as we shall soon see, is strongly tied to the *Green's function* or *propagator* of the system - a highly useful and often employed theoretical tool. It should be noted that the actual photocurrent as measured may have additions to these terms - resolution effects and a background from secondary scattering are possible complexities.

1.3.2 The spectral function

The one-electron removal probability in Equation 1.9 described above is, in essence, the *spectral function.* Specifically it is the single particle removal spectral function. Soon we will see how this is tied to the Green's function formalism, but first the concept of a *quasi-particle* needs a more intimate introduction.

Quasi-particles

A *quasi-particle* is, as its name implies, almost a particle, but not quite. For most intents and purposes, a quasi-particle is a term used to wrap up a lot of unnecessary detail into something which can be treated like a particle. The standard example is a particle moving through a medium with which it can interact.

In a medium where interactions are possible a particle will, needless to say, interact. Whether the interactions are with other particles or *collective excitations* like phonons (quantized lattice vibrations) and magnons (quantized spin waves)[1] the particle will have an effect on the system and the system an affect on the particle.

Describing the motions of each individual in these interactions would be difficult (in many instances one might claim, impossible) however, often, the particle and interactions with the system can together be easily described as a quasi-particle.

As an example we take an electron moving through a lattice under the influence of an electric field. As it travels it interacts with the lattice, constantly creating and destroying phonons in a cloud around itself. The actual dynamics of the individual electron and phonons can be quite complicated, however by considering the group as a whole we may ignore these complications and still study the behaviour of the system. This system as a whole - the *bare particle* (electron, in this case) plus *dressing* (lattice excitations) together make up the quasi-particle.

[1] or even fluctuations of virtual particles in the vacuum

Although describing the dynamics of electrons and phonons in this system would be a total nightmare, one finds that for certain energies and momenta there exist quasi-particles which move through the lattice with an *effective mass* and, in general, have a finite *lifetime*.

An often defined quantity for these quasi-particles is the *self-energy*. This is simply the 'new' energy acquired by the quasi-particle due to its dressing.

$$\epsilon_{\text{quasi particle}} - \epsilon_{\text{bare particle}} = \epsilon_{\text{self}} \equiv \Sigma \tag{1.10}$$

This self-energy, a complex quantity, represents both the change in energy (the real part) as well as the finite lifetime (the imaginary part) of the quasi-particle.

Green's functions

Now that the quasi-particle has been introduced, we move on to a brief introduction to the *Green's function* formalism. For many, even amongst physicists, talk of Green's functions or *propagators* is accompanied by a quick visual inspection of the room in an attempt to judge whether or not undetected escape is possible. Sadly, especially for those of us fortunate enough to actually do ARPES, this causes many to miss out on the beautiful connection between ARPES, the spectral function, and the Green's function (hereafter called simply the propagator to reduce the intimidation). For readers interested in a thorough introduction to the propagator I highly recommend Mattuck's book: *A Guide to Feynman Diagrams in the Many-Body Problem* [21], which brings the problem to a level accessible to mortal grad students. This section will clarify the use of the single-particle propagator as far as necessary to make the aforementioned connections, but my goal is not to produce a substitute for an entire book.

Classical Propagator We start with the idea of a *classical propagator*. In many simple examples, the kind that are solved in undergraduate mechanics courses, special functions are not needed to describe the propagation of a particle.

For example, we can describe the propagation to position r_2 at time t_2 of a particle initially at rest at position r_1 at time t_1 subjected to a constant force through the familiar expression:

$$r_2 - r_1 = \frac{F}{2m}(t_2 - t_1)^2 \tag{1.11}$$

However, if we complicate the system - say by allowing the particle to collide with other objects (allowing, ahem, interactions) perhaps the best we could do would be to describe the *probability density*, $P(r_2, t_2, r_1, t_1)$, that a particle get carried from position r_1 at time t_1 to position r_2 at later time t_2. This would then be a classical propagator.

Quantum Propagator The idea of a *quantum propagator* is not so different from that of a classical one. The main differences all stem from the fundamental differences between classical and quantum descriptions.

First, the propagator, G, describes not the probability density but a *probability amplitude*, thus when calculating the probability density $|G|^2 = G^*G$ one finds interference terms if G was expressed as a sum of smaller propagators (as usual with quantum processes).

More importantly to our study here, we should not think of propagation between positions $r_1 \rightarrow r_2$ but states described by a full set of quantum numbers $k_1 \rightarrow k_2$[2]. Also, as is always the case for indistinguishable particles, it is impossible to say a specific electron propagates from k_1 to k_2. The best we can say is that, at time t_1 there was *an* electron in state k_1 and at t_2 there was *an* electron in state k_2.

Thus we describe the quantum propagator, $G(k_2, k_1, t_2 - t_1)$, for $t_2 > t_1$ as the probability amplitude that if at time t_1 we add a particle in some state expressed by quantum numbers k_1 to an interacting system in its ground state, then check again at time t_2 we find the system again its ground state with a particle in state k_2. For all possible times $t_2 - t_1$, G may then be written (simply by its definition) as [21]:

$$G(k_2, k_1, t_2 - t_1) = -i \langle \Psi_0 | \mathcal{T} \left[c_{k_2}(t_2) c^\dagger_{k_1}(t_1) \right] | \Psi_0 \rangle \tag{1.12}$$

Where $\mathcal{T}[\,]$ is the Wick time-ordering operator, and $c^\dagger_k(t)/c_k(t)$ are the creation/annihilation operators for a state described by k at time t. With the eventual goal of deriving the spectrum we begin by expanding the time-ordering operator for Fermions:

$$G(k_2, k_1, t_2 - t_1) = \begin{cases} G^+(k_2, k_1, t_2 - t_1) = -i \langle \Psi_0 | c_{k_2}(t_2) c^\dagger_{k_1}(t_1) | \Psi_0 \rangle & , t_2 > t_1 \\ G^-(k_2, k_1, t_2 - t_1) = +i \langle \Psi_0 | c^\dagger_{k_1}(t_1) c_{k_2}(t_2) | \Psi_0 \rangle & , t_2 \leq t_1 \end{cases} \tag{1.13}$$

[2]Here I have written k, which generally implies momentum (as that will be the quantity we care about most in the following discussion). However, this k truly represents all the quantum numbers we need to describe the states we are interested in.

Here we see the aforementioned case for $t_2 > t_1$ as well as G^- for $t_2 \leq t_1$ which can be interpreted as the *hole* propagator from time t_2 to t_1.

As our goal is to develop something similar to the spectral function as observed by ARPES (Equation 1.9), we now examine the case where $k_1 = k_2 \equiv k$ and set $t_1 = 0$, $t_2 = t$. Expanding G^- for an N particle system using the Heaviside step function, $\Theta(t)$ and Heisenburg picture for operators $c_k(t)^{\pm} \rightarrow e^{iHt} c_k^{\pm} e^{-iHt}$ we find:

$$G^-(k,t) = i\Theta(-t) \left\langle \Psi_0^N \right| c_k^\dagger \; e^{iHt} c_k e^{-iHt} \left| \Psi_0^N \right\rangle \tag{1.14}$$

To this, we insert the identity operator $\sum_{n,N'} \left| \Psi_n^{N'} \right\rangle \left\langle \Psi_n^{N'} \right|$ (wherein only the $N' = N - 1$ term will survive)

$$\begin{aligned} G^-(k,t) &= i\Theta(-t) \sum_n \left\langle \Psi_0^N \right| c_k^\dagger e^{iHt} \left| \Psi_n^{N-1} \right\rangle \left\langle \Psi_n^{N-1} \right| c_k e^{-iHt} \left| \Psi_0^N \right\rangle \\ &= i\Theta(-t) \sum_n \left| \left\langle \Psi_n^{N-1} \right| c_k \left| \Psi_0^N \right\rangle \right|^2 e^{i(E_n^{N-1} - E_0^N)t} \end{aligned} \tag{1.15}$$

Taking the Fourier transform over time $G^-(k,\omega) = \mathcal{F}\left[G^-(k,t)\right]\ldots$

$$G^-(k,\omega) = \sum_n \frac{\left| \left\langle \Psi_n^{N-1} \right| c_k \left| \Psi_0^N \right\rangle \right|^2}{\omega + (E_n^{N-1} - E_0^N) - i\delta} \tag{1.16}$$

With large volume systems[3] the energy levels will be so closely spaced that we may express G^- as an integral through the introduction of the *spectral function*, $A(k,\omega)$:

$$G^-(k,\omega) = \int_0^\infty \partial\omega' \frac{A^-(k,\omega')}{\omega + \omega' + i\delta} \tag{1.17}$$

Where

$$A^-(k,\omega) = \sum_n \left| \left\langle \Psi_n^{N-1} \right| c_k \left| \Psi_0^N \right\rangle \right|^2 \delta\left(\omega + (E_n^{N-1} - E_0^N)\right) \tag{1.18}$$

On comparing this spectral function with Equation 1.9 we notice that, if we set matrix elements to unity, we are directly probing the spectral function with ARPES by measuring $A^-(k, E_k^{e^-} - h\nu)$. Let's take a minute to think about this... We were looking at the propagator, a measure of

[3] all systems studied by ARPES are large on the quantum scale

how expectation values in a system change over time - an especially useful description *even if the system includes unsolvable correlation effects.* From this we found the spectral function - a quantity we can directly measure through Angle Resolved Photoemission. Amazing.

Self-energy

As stated earlier (see Equation 1.10) one of the of the tools in examining electronic correlations is the *self-energy*, Σ of a quasi-particle. Simply put, it is the additional energy of a particle due to interactions with a system.

For reasons well beyond the scope of this thesis (see, again, Mattuck's excellent book [21]) the calculation of this complex self-energy through summation of Feynmann diagrams turns out to be an excellent and convenient method of calculating the aforementioned Green's function (and, often, the only method possible) through the relationship:

$$G(k,\omega) = \frac{1}{\omega - \epsilon_k - \Sigma(k,\omega) + i\delta} \tag{1.19}$$

Where ϵ_k is the band structure which would exist without correlation effects. ARPES experimentalists would naturally like to see how this self-energy relates to our measurable quantity, the spectral function. Although it was omitted earlier G^+ may be constructed from A^+ in a manner similar to Equation 1.17, thus giving the full Green's function:

$$G(k,\omega) = \int_0^\infty \partial\omega' \left[\frac{A^+(k,\omega')}{\omega - \omega' + i\delta} + \frac{A^-(k,\omega')}{\omega + \omega' + i\delta} \right] \tag{1.20}$$

Using complex function theory (see ref. [5]) we may evaluate this integral to discover:

$$\begin{aligned} A^+(k,w) &= -\tfrac{1}{\pi}\mathrm{Im}\left[G(k,\omega)\right], \quad \omega > 0 \\ A^-(k,-w) &= +\tfrac{1}{\pi}\mathrm{Im}\left[G(k,\omega)\right], \quad \omega < 0 \end{aligned} \tag{1.21}$$

Since A is the imaginary part of the Green's function we may multiply Equation 1.19 by the complex conjugate of the denominator and take the imaginary part to find the spectral function in terms of the real and imaginary parts of the self-energy:

$$\begin{aligned} A^+(k,\omega) &= -\tfrac{1}{\pi} \frac{\mathrm{Im}[\Sigma(k,\omega)]}{(\omega - \epsilon_k - \mathrm{Re}[\Sigma(k,\omega)])^2 + (\mathrm{Im}[\Sigma(k,\omega)])^2} \\ A^-(k,-\omega) &= \tfrac{1}{\pi} \frac{\mathrm{Im}[\Sigma(k,\omega)]}{(\omega - \epsilon_k - \mathrm{Re}[\Sigma(k,\omega)])^2 + (\mathrm{Im}[\Sigma(k,\omega)])^2} \end{aligned} \tag{1.22}$$

This allows us, albeit somewhat indirectly, to measure the particle self-energy through ARPES. As stated earlier the self-energy is a measure of correlation effects and quasi-particle properties. The real part, as can be seen from Equation 1.10, is a measure of the quasi-particle energy renormalization. The imaginary part is a measure of the quasi-particle lifetime.

Chapter 2

The Holstein polaron

In order to study real life correlated systems, a foundation must be laid by examining theoretical models. Even the simplest of models can hold valuable insights. Often, in fact, the simplest models hold the most valuable insights because they allow a study more focused on the desired properties, uncluttered by excess detail.

In the most general sense the term *polaron* describes a quasi-particle due to interactions with a bosonic environment. The *Holstein polaron* [11] is the simplest example in a long list of possible polaron models. It is based on an on-site coupling of electrons to a dispersionless phonon mode and can be described by the Hamiltonian [8]:

$$H = \sum_k \epsilon_k c_k^\dagger c_k + \Omega \sum_q b_q^\dagger b_q + \frac{g}{\sqrt{N}} \sum_{k,q} c_{k-q}^\dagger c_k (b_q^\dagger + b_{-q}) \qquad (2.1)$$

Here $c_k^\dagger$ and c_k are the creation/annihilation operators for electrons with bare-particle dispersion ϵ_k. $b_q^\dagger$ and b_q are the creation/annihilation operators for dispersionless optical phonons possessing an energy Ω regardless of momentum, q. The final term is the on-site electron-phonon coupling of strength g, transformed into momentum-space over N lattice sites.

The Holstein polaron is a long standing problem, with analytic descriptions existing only at the extreme edges of parameter space[4]. However, it is known that the solution (whatever it may be) is analytic over the entire parameter space, ensuring a smooth crossover between the known regimes [18]. There has also been much numerical work done (see [8, 20], for some examples) in an attempt to describe this transition. The work done on these model systems is invaluable in attempting to explain the observations of real life correlated systems.

Chapter 3 examines, in detail, the Holstein polaron problem through the tools accessible to ARPES. This will allow a greater understanding not only of this particular system, but more importantly, broader quasi-particle behaviours and the possibilities of ARPES data analysis in general.

[4] until the introduction of the momentum average approximation, discussed in § 2.2

In order to first get a feel for the model and subsequent analysis, this chapter will study the qualitative behaviour of the model. This will be done through known behaviour in the low and high coupling limits, as well as through the spectral function produced by Mona Berciu's momentum average approximation[2] as implemented by her student, Glen Goodvin, in their recent study of the Holstein polaron[3].

2.1 Solutions

2.1.1 Low coupling limit

At the absolute end of the low coupling limit, the 'quasi-particle' is merely an electron with no dressing whatsoever. Therefore, it simply follows the bare band structure. When coupling is turned on a continuum of possible quasi-particle arrangements becomes available. This continuum will essentially be the bare band, shifted in energy and momentum by the integer number of phonons in the quasi-particle (see Figure 2.1). This causes a disturbance to appear at the phonon energy and a spreading out of those states of higher energy which have access to the new continuum.

As coupling increases the continuum of states quickly becomes overwhelming, and a quasi-particle description in this region becomes invalid. For this reason, when studying this system (and many others) it is common to call the first peak *the* quasi-particle and the rest *the* continuum. This nomenclature is used for all couplings in the low coupling limit.

2.1.2 High coupling limit

In the high coupling limit there are many phonons in the polaron quasi-particle due to the strong interaction. This suppresses the polaron motion, as the electron must drag with it a large phonon cloud. Since the polaron is then essentially localized in real-space it must be delocalized in momentum-space. In this case, the energy will depend on the number of phonons, thus in the high coupling limit the spectrum is a ladder of states separated by the phonon energy.

2.1.3 Transition regime

The transition between these two limits is worthy of qualitative discussion. Starting from the bare band we turn on coupling and arrive in the low coupling limit. As described in the low coupling limit a quasi-particle peak splits

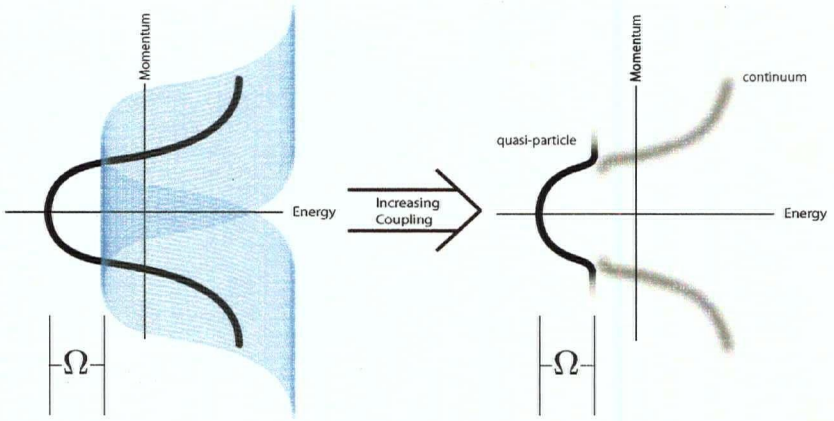

Figure 2.1: The quasi-particle energy-momentum relation in the low coupling limit. When coupling is turned on a continuum of new quasi-particle states becomes available as an electron coupled to an integer number of phonons. Pictured here, in black, is the bare band dispersion. In blue is the portion of the continuum of quasi-particles states becoming available which consist of a single electron and phonon combination. These new states are simply the bare band dispersion translated by phonon energy, Ω, and phonon momentum. Since the phonon is dispersionless, its momentum is arbitrary and the result is a continuum smeared out over all possible momenta. This newly available continuum modifies the bare band dispersion, causing a disturbance and redistribution of weight beginning at the phonon energy. This continuum region quickly becomes very broad, and inside it a quasi-particle description looses its utility. For this reason *the* quasi-particle peak generally refers to the first, coherent, region and *the* continuum refers to the rest of the broad distribution.

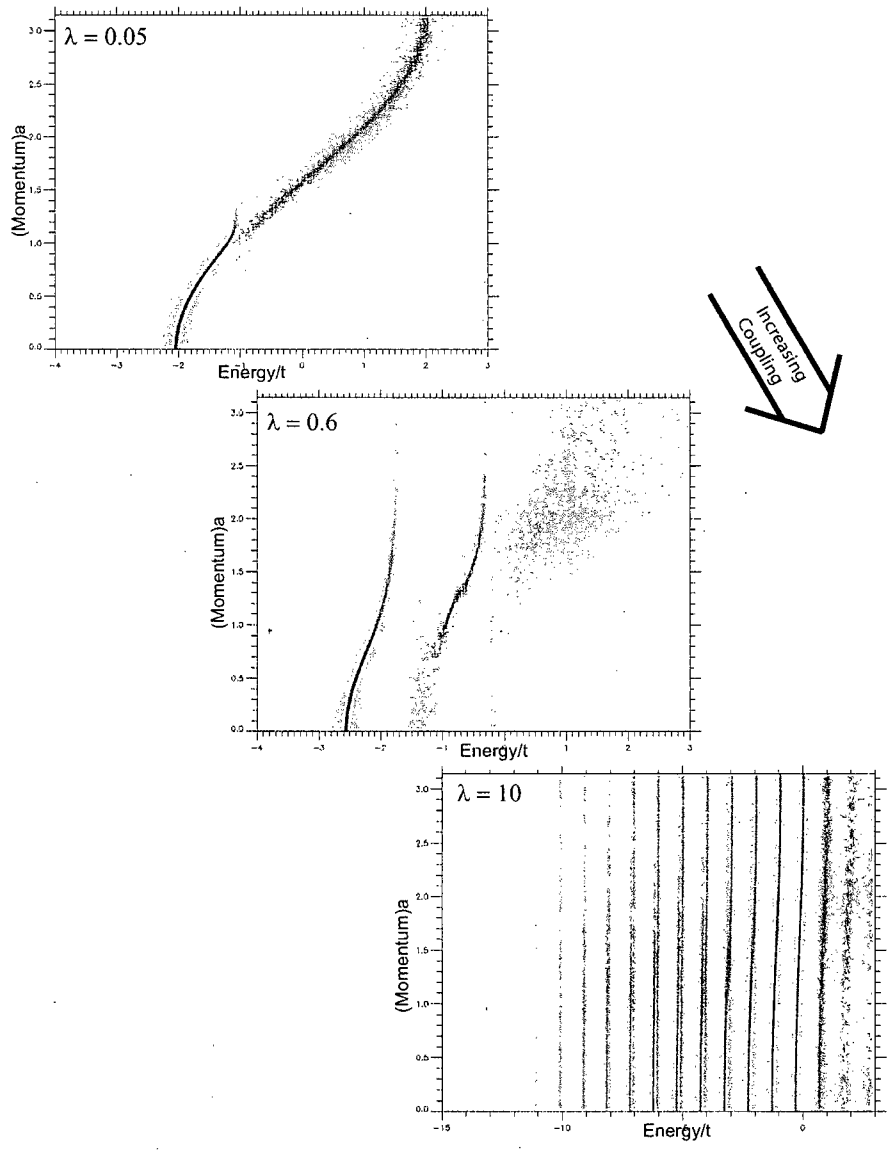

Figure 2.2: When coupling is first turned on a quasi-particle splits off from the continuum via the method seen in Figure 2.1. As coupling is increased the system smoothly develops into the high coupling limit; a ladder of states separated by the phonon energy. Here we see the spectral function as derived in [8] for $\lambda = 0.05, 0.6, 10$.

off from the continuum. The character of this quasi-particle changes with both momentum and coupling strength. As coupling increases the quasi-particle will have a larger phonon cloud due to the stronger interactions. Also, the sharp flattening in the quasi-particle dispersion relation seen in Figure 2.1 and Figure 2.2, upper panel, is due to increasing quasi-particle effective mass as more phonon interactions becoming available. Thus a larger phonon cloud is also present at high quasi-particle momenta.

As coupling is increased further, the quasi-particle takes on a progressively larger phonon cloud, increasing its weight and narrowing its bandwidth. At the same time, the weight in the continuum starts to stratify at intervals of the phonon energy through the same mechanism seen in Figure 2.1.

With higher coupling this stratification continues and the continuum inbetween phonon energies becomes progressively smaller as the spectrum asymptotically approaches the ladder of states separated by the phonon energy as in the high coupling limit. See Figure 2.2.

2.2 Momentum average approximation

With the recently introduced momentum average (MA) approximation[2] the Holstein polaron can now be studied with a speed and accuracy not previously possible. For this reason, it has been used as the exclusive model on which to test this new method of spectral function analysis. What follows is a qualitative introduction to the model, and a description of the parameters employed.

As previously discussed the calculation of a quasi-particle's self-energy through the summation of Feynmann diagrams is an often-used tool. There are, in general, an infinite number of diagrams for any system. In rare cases one might be lucky enough that the diagrams can be expressed by a known infinite series, however these instances exist for only a few textbook examples. Many methods exist to bypass this problem. Most analytic methods involve making some approximation whereby certain types of diagrams are ignored allowing a sum to be carried out over certain parameter regimes. Numerical methods exist as well, Quantum Monte Carlo methods [20], for example, have traditionally formed the main effort to study the problem over a wide range of parameters. However, they are computationally expensive.

The MA(n) method involves summing all self-energy diagrams, made possible by averaging each diagram over the momenta of its free propagators. Any number of propagators can be left in their true (not averaged)

form, but this increases computation time. The index n refers to highest order propagator left exact, specifically it is how many phonons it contains. For this thesis MA(1) was used. It is both highly accurate and computationally efficient, allowing a sampling of the spectral function at a resolution previously impossible. Goodvin has provided the source code for his software used to generate data for his recent paper with Berciu, allowing the study of the Holstein polaron with the same software tools designed by me for ARPES analysis.

The description of the Holstein polaron used here assumes nearest neighbor hopping on a 1D lattice of spacing a, with $\hbar$ set to one. With hopping parameter t the bare electronic dispersion becomes:

$$\epsilon(k) = -2tcos(ka) \tag{2.2}$$

The coupling is described in terms of the dimensionless parameter λ defined as:

$$\lambda = \frac{g^2}{2t\Omega} \tag{2.3}$$

2.2.1 Comparison to ARPES data

In the system studied here the ground state, Ψ_0, is the vacuum. For this reason it is only possible to observe the interactions by the addition of an electron and the quantity calculated is A^+ - the standard for both analytic and numerical simulations.

In ARPES we measure A^-, the electron removal spectrum. In this case, because there are no electrons, ARPES would be impossible[5]. However, this distinction does not affect the study of the spectral function and its relationship to the self-energy. The difference manifests itself only as a change in sign of the energy. For this reason the positive direction in energy on all figures generated in the following discussion is reversed to what one would expect to see in a photoemission experiment.

Also, all energies are expressed relative to the hopping energy, t and momenta to the inverse lattice constant, $\frac{1}{a}$.

[5] Although angle resolved *inverse* photoemission has been performed, it is not as widely used due to a comparative lack of resolution and larger technical difficulties

Chapter 3

Spectral Function Analysis

Here we take the Holstein polaron spectral function calculated via the momentum average approximation in [8] and examine it using the tools generally applied to ARPES. Since all parameters and functions are known, this makes for an excellent opportunity to study not just the system, but also the tools used.

3.1 Self-energy and MDC analysis

As we have seen, under ideal circumstances, ARPES measures the *spectral function.* As one might imagine, this is an extremely rich source as it contains information on all possible interactions within the system. Assuming all the experimental considerations and difficulties discussed previously have been eliminated, and the spectral function has been resolved perfectly over some experimental window[6], one might ask: Now what?.

If one is trying to fit data to a model for which the spectral function is known, one might imagine an iterative process whereby the parameters of the model are adjusted and the results compared to the experimental spectral function collected (see, for example [13]).

Under some circumstances if the complete model, or even the entire underlying bare band structure, is unknown one may fall back on a powerful technique known as Momentum Distribution Curve (MDC) analysis. Through this method it is possible to uncover both the bare band electronic structure as well as the real and imaginary parts of the self-energy, within certain restrictions, as discussed below.

3.1.1 MDC analysis

This method hinges on the self-energy being *momentum independent.* The MA approximation to the Holstein polaron problem does yield a momentum independent self-energy, making it an excellent candidate to demonstrate the technique.

[6] a formidable task in and of itself

The method outlined here varies slightly from techniques previously described in the literature, which often deal with data very close to the Fermi surface and generally reduce the possible functional forms for the bare band structure substantially (see, for example, Ref. [17]). This route was taken after attempting multiple techniques, whereby it was found that not making assumptions about the functional form of the bare band structure allowed for a much more accurate result.

In this technique we examine the spectral function along lines of constant energy, the so-called Momentum Distribution Curves. Examining Equation 1.22 with a momentum independent self-energy, we discover that for a constant energy, $\tilde{\omega}$, the function described is remarkably similar to that of a Lorentzian:

$$A_{\tilde{\omega}}(k) = -\frac{1}{\pi}\frac{\mathrm{Im}\left[\Sigma_{\tilde{\omega}}\right]}{\left(\tilde{\omega} - \epsilon(k) - \mathrm{Re}\left[\Sigma_{\tilde{\omega}}\right]\right)^2 + \left(\mathrm{Im}\left[\Sigma_{\tilde{\omega}}\right]\right)^2} \tag{3.1}$$

$$\mathrm{Lorentzian}(x) = \frac{1}{\pi}\left(\frac{\gamma}{(x - x_0)^2 + \gamma^2}\right) \tag{3.2}$$

Here we see that the Spectral function will have a maximum at $\tilde{\omega} - \epsilon(k) - \mathrm{Re}\left[\Sigma_{\tilde{\omega}}\right] = 0$ and a Half Width Half Maximum (HWHM) proportional to $\mathrm{Im}\left[\Sigma_{\tilde{\omega}}\right]$. This means that to extract the self-energy we must use the bare band dispersion ϵ_k which is, of course, unknown. To this end we expand ϵ_k about the location of the maximum in $A_{\tilde{\omega}}(k)$, $k = k_m$ using primes to notate the derivative with respect to momentum.

$$\epsilon(k) = \epsilon(k_m) + \epsilon'(k_m) \cdot (k - k_m) + \ldots \tag{3.3}$$

Where k_m is the momentum at the maximum in the MDC, the momentum required to make the denominator in Equation 3.1 as small as possible:

$$\epsilon(k_m) = \tilde{\omega} - \mathrm{Re}\left[\Sigma_{\tilde{\omega}}\right] \tag{3.4}$$

Which allows us to write the Taylor series as:

$$\epsilon(k) = \tilde{\omega} - \mathrm{Re}\left[\Sigma_{\tilde{\omega}}\right] + \epsilon'(k_m) \cdot (k - k_m) + \ldots \tag{3.5}$$

Substituting our truncated Taylor series for $\epsilon(k)$ we may re-write Equation 1.22 in a more provocative way:

$$A_{\tilde{\omega}}(k) = -\frac{1}{\pi}\frac{\frac{\mathrm{Im}[\Sigma_{\tilde{\omega}}]}{\epsilon'(k_m)}}{(k - k_m)^2 + \left(\frac{\mathrm{Im}[\Sigma_{\tilde{\omega}}]}{\epsilon'(k_m)}\right)^2} \tag{3.6}$$

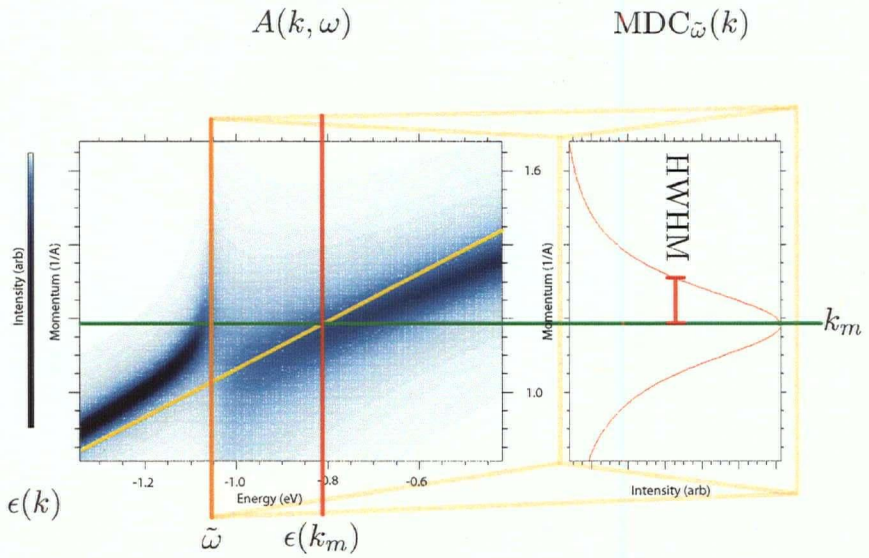

Figure 3.1: Equation 3.7 described diagrammatically. From the spectral function an MDC is taken at energy $\tilde{\omega}$ (orange highlight). Within the limits discussed this MDC will have Lorentzian form, with some maximum denoted k_m (marked in green). From the nature of the bare electronic band structure (yellow) evaluated at k_m and the MDC fitting parameters we may extract the real and imaginary parts of the spectral function at $\tilde{\omega}$

And so we see that for every energy there should be an MDC which has Lorentzian form, provided the self-energy is momentum independent and that a first order Taylor series to the bare band is accurate in the neighborhood of k_m. From a Lorentzian fit of these MDCs we could retrieve the energy-dependent self-energy through:

$$\begin{aligned} \mathrm{Im}\left[\Sigma_{\tilde{\omega}}\right] &= -\left[\mathrm{HWHM} \cdot \epsilon'(k_m)\right]_{\tilde{\omega}} \\ \mathrm{Re}\left[\Sigma_{\tilde{\omega}}\right] &= \left[\tilde{\omega} - \epsilon(k_m)\right]_{\tilde{\omega}} \end{aligned} \tag{3.7}$$

Where k_m, defined by $\epsilon(k_m) = \tilde{\omega} - \mathrm{Re}\left[\Sigma_{\tilde{\omega}}\right]$, is easily measured as the momentum location of the maximum in intensity. This relation, however, requires knowledge of the bare band dispersion $\epsilon(k)$.

3.1.2 Known band results

Postponing the problem of tackling the unknown band dispersion for the moment, a natural first question would be - if the band structure is known, does the scheme described in Equation 3.7 work as advertised?

Assuming we stick to areas where the (known) band dispersion is well approximated by its first-order Taylor series (ie. away from maxima and minima) the approximations should be valid for our test system, as the MA approximation to the Holstein polaron model does indeed have a momentum-independent self-energy. The only major issue, then, is one of numerics: The spectral function, especially at low coupling, has regions where it could well be approximated by a Dirac δ function. An infinitesimally thin, infinitely tall, function can not be represented numerically - thus some broadening must be applied. In these simulations a Lorentzian broadening is applied in energy only, something which might be considered similar to an impurity scattering broadening.

This broadening will, of course, cause some weight from different momenta to mix, causing an effective broadening in the momentum direction as well. To first order, the ratio of this effective momentum broadening to the intended energy broadening will come from the slope of the dispersion relation - the band velocity. Initially this varying contribution seems troubling, however as seen in Equation 3.7, the band velocity also determines the ratio between $\mathrm{Im}\left[\Sigma_{\omega}\right]$ and the MDC HWHM. Fortunately, as Lorentzian HWHMs add under convolution, this shows up as a constant offset once the HWHM has been converted to $\mathrm{Im}\left[\Sigma_{\omega}\right]$ according to 3.7 and can be subtracted directly.

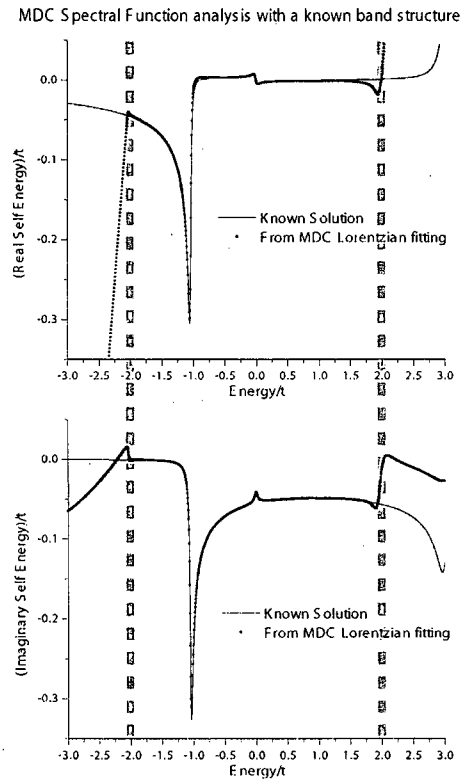

Figure 3.2: Here the model spectral function ($\Omega = 1.0$, $\lambda = 0.05$) was examined with Equation 3.7 to retrieve the real and imaginary parts of the spectral function. The band structure was taken as known, so the relationship is trivial in areas where both the Taylor series approximation to the band structure is valid, and where MDC Lorentzian fits can be based on adequate, relevant, spectral weight. The dashed line marks the outside of this region, which (so close to the low-coupling limit) is essentially the area covered by the bare band dispersion.
The fitting machinery was applied to the entire energy window, to demonstrate it's failure outside this region. One can see that it first begins to fail close to the band edges, where the band velocity $\frac{\partial}{\partial k}\epsilon(k)$ goes to zero and the Taylor series becomes invalid. Once outside the band all spectral weight is purely from energy broadening and the results are totally invalid.

Performing this prescription, for low coupling, produces excellent results. As can be seen in Figure 3.2 where there is spectral weight to fit, both the real and imaginary parts of the self-energy are reproduced almost exactly. Outside the region with spectral weight (in this case, near the low coupling limit, this is essentially the bare electronic band) the spectral weight is purely due to the energy broadening, and so the machinery produces invalid results.

As coupling is increased the fit improves initially, as the effects due to energy broadening (which are only corrected to first order) and finite sampling effects become smaller compared to the self-energy broadening. After a point, however, the loss in spectral weight experienced as the quasi-particle state splits away from the continuum[7]takes its toll and the MDC fits are compromised by loss of spectral weight. The failure of MDC analysis should not be surprising at these large couplings, as the MDC widths (still dictated by Equation 3.6) quickly surpass the size of the Brillouin Zone. This progression can be seen in Figure 3.3.

3.1.3 The Kramers-Kronig relations

We saw in the last section that, given the band dispersion, it is possible to extract the self-energy. However, in real life,[8] we don't necessarily know the bare electronic dispersion. While it is often possible to calculate the dispersion via Density Functional Theory (DFT) (typically under the Local-Density Approximation (LDA) [22]), questions about the validity of these calculations when faced with uncertain doping or surface re-construction are often raised. Ideally, it would be possible to reconstruct everything from the spectral function alone.

In order to do this, more information than the relationships given in Equations 3.7 would be required. Fortunately, there is a relationship between the real and imaginary parts of the self-energy. In principle the *Kramers-Kronig* relations open the way to extract both the self-energy and the bare band from the spectral function.

[7]Spectral weight is, naturally, never lost completely as that would violate particle conservation. The weight loss observed at the energy directly inbetween quasi-particle and continuum has simply been shifted to other energies. It is worth noting that spectral weight can not be shifted between different momenta, as every value of momentum must have constant total spectral weight (unity, if it has been properly normalized)[4]. This is an extension the bare band picture where energy is a function of momentum, to the interacting picture where the expected energy for a given momentum can be spread out but not destroyed.

[8]Experimental life, that is!

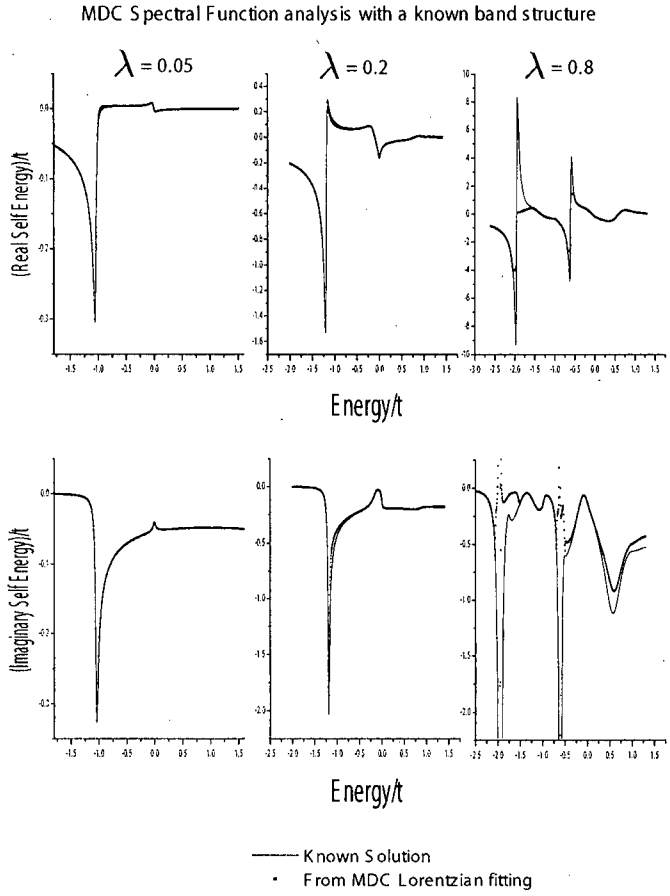

Figure 3.3: Real and imaginary parts of the self-energy, as found by examining MDC Lorentzian fits using the known band structure. Here we see that as coupling is increased fit is still good, but once the imaginary part of the spectral function becomes too large (note the changing energy scale) the MDC peak width becomes larger than the Brilliouin zone, and the Lorentzian fitting fails, causing gaps where the self-energy is no longer resolved. $\Omega = 1.0$ for all panels.

The Kramers-Kronig relations are relationships between the *Hilbert transforms* of the real and imaginary parts of a complex function, and applies to the self-energy as follows: As the complex frequency dependent response function of a causal system, the self-energy must be both analytic in the upper half plane and vanish at infinity [14, 16]. As such we may consider the following integral over the upper half plane, excluding the origin, for any constant k:

$$\oint \partial\omega' \frac{\Sigma(k,\omega')}{\omega' - \omega} = 0 \tag{3.8}$$

This may be evaluated leaving just the contributions from the real axis and the hump over the origin. These may be re-arranged to give the Kramers-Kronig relation in its familiar form:

$$\Sigma(k,\omega) = \frac{1}{i\pi}\mathcal{P}\int_{-\infty}^{\infty} \partial\omega' \frac{\Sigma(k,\omega')}{\omega' - \omega} \tag{3.9}$$

Where $\mathcal{P}$ is the Cauchy principal value of the integral. Or as it is more often seen in ARPES literature:

$$\begin{aligned} \mathrm{Re}\left[\Sigma(k,\omega)\right] &= +\frac{1}{\pi}\mathcal{P}\int_{-\infty}^{\infty} \partial\xi \frac{\mathrm{Im}\left[\Sigma(k,\xi)\right]}{\xi - \omega} \\ \mathrm{Im}\left[\Sigma(k,\omega)\right] &= -\frac{1}{\pi}\mathcal{P}\int_{-\infty}^{\infty} \partial\xi \frac{\mathrm{Re}\left[\Sigma(k,\xi)\right]}{\xi - \omega} \end{aligned} \tag{3.10}$$

Using this relationship we may, in principle, determine both the bare band and the self-energy from the spectral-function. In practice this has already been done by choosing a form for the bare band (usually linear [15] or quadratic [17]) and modifying the parameters until the best self-consistency is reached after performing the KK transform.

3.1.4 Kramers-Kronig results

Again postponing difficulties until later, we first investigate conditions under which the Kramers-Kronig transforms will successfully transform between real and imaginary parts, when all other things are known.

The first problem is that of tails. One will notice that the integrals in Equation 3.10 run over all energies from $-\infty \rightarrow +\infty$. Real life experimental windows aside, as we saw in § 3.1.2, even with access to the spectral function over an unlimited range in energy our knowledge of the self-energy is still limited to areas with adequate spectral weight.

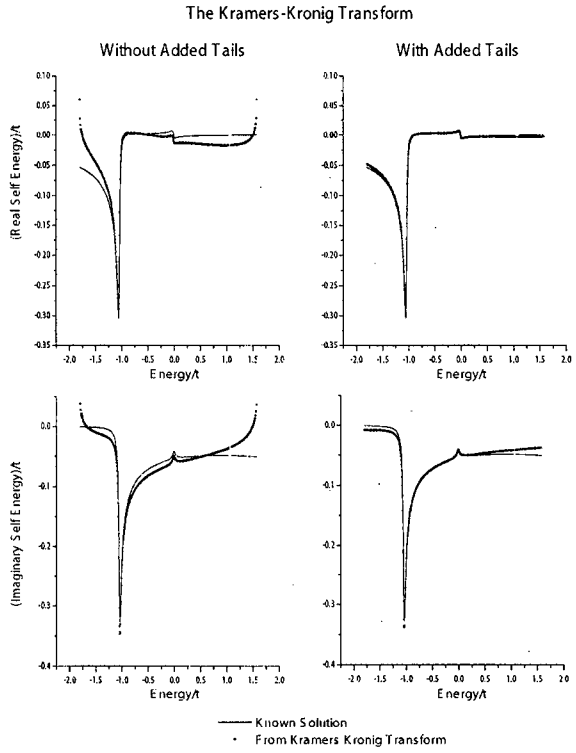

Figure 3.4: The Kramers-Kronig Transform on a finite data set, performed with and without the addition of tails to the data. This figure demonstrates the importance of using an appropriate tail when implementing the Kramers-Kronig transform. The data is from the same set as used in Figure 3.2, cropped to the best known energy window. For the left panel the KK transforms were blindly applied to get the real self-energy from the MDC imaginary self energy (upper panel), and the imaginary self-energy from the MDC real self energy (lower panel). For the right panel an inverse polynomial fit was used to add tails before the KK transforms were performed, and the transformed data set truncated back to original size. Without the addition of a tail the fit is poor, especially near the endpoints.

In order to evaluate the Kramers-Kronig relations a fourier series method was used, similar to that described in Reference [14], as implemented by the native `Hilbert()` function in the programming language IDL 6.3. It involves taking the Fast Fourier Transform (FFT), shifting the first half of the transform products by +90 degrees and the second half by -90 degrees, then taking the FFT again to put it back in energy space. Due to this a tail is not strictly required in order to evaluate the integral, however the results are poor. In Figure 3.4 the results of attempting the Kramers-Kronig transform with and without the addition of approximated tails are shown.

Another problem, although easily solved, in that of a constant offset. Equation 3.10 reveals that the Kramers-Kronig transformed are only unique to within a constant offset. This can be remedied by shifting the KK transformed functions such that their mean values are the same as the measured functions before comparison. The original MDC measured self-energies should not be shifted, as this would change the measured function of interest!

In order to solve the problem of tails I used fits to a negative power series, the center discontinuity of which was permitted to drift. A separate fit was done for each side, where the weighting of data points on the fit decayed exponentially with distance from the edge. I found that the best results were obtained by a fourth order fit. Although this procedure gave better results than polynomial or exponential fits, the possibilities have been by no means exhausted and there are certainly improvements which could be made. As seen in Figure 3.4 it has greatly improved the accuracy of the transform, although not fixed it entirely.

3.1.5 Band unknown results

Based on the foundation set above, the final question is - can we extract everything from the spectral function alone? Without knowledge of the bare band can we decompose Equation 3.7 into the Bare Band dispersion ϵ_k as well as real and imaginary parts of the self-energy using the KK relations (Equation 3.10) as a guide?

The answer, under certain situations and limitations, is yes.

Limitations

The first limitation is that of a total energy offset. An examination of Equation 3.7 shows us that for a given ω the real part of the self-energy is simply the difference between the bare band at k_m and ω. Also, as discussed

in § 3.1.4, Equation 3.10 only relates real and imaginary parts of the self-energy to within a constant offset. For this reason, we should at best only expect to be able to extract the real part of the self-energy to within a constant offset of its true form.

The situations under which it can work are, of course, also limited to those situations discussed in the previous sections which place limits on the individual steps. The spectral function must be known in a regime where MDC Lorentzian fits will give meaningful results.

Band structure model

Under these limitations, however, we see reasonable results. In these tests a polynomial band structure of adjustable degree was used. A first 'guess' at the band structure was made by fitting the Lorentzian maxima alone. Based on this band structure the real and imaginary parts of the self-energy are calculated via Equation 3.7, and their KK transforms compared. The coefficients of the bare band structure are then adjusted with the goal of reducing the difference between the self-energy from both sources (MDC and MDC→KK).

Due to the wide energy range taken, and the subsequent range of band structure required, it was found that in most circumstances a polynomial of at least third order was required in order to get reasonable results. Best results were found between third and seventh order depending on how large an energy window was taken. The lower limit on which order to choose comes from how sensitive the real part of the self-energy is to slight deviations in actual band to the fit band. In order to accurately determine a real self-energy on the order of $0.01t$, the model must be capable of matching the band to well under this value over the entire length. With a large data set, it was found to be simply impossible to fit the bare band accurately enough.

The upper limit stems from the same sensitivity, and must be limited in order to keep oscillations in the fit band from forming.

Results

Once the fitting is as self consistent as possible the closest results always come from the MDC imaginary self-energy. This is because it depends only on the derivative of the polynomial band structure, which is more tightly constrained. So for the most reliable results, one should use the MDC imaginary self-energy and the KK real self-energy derived from it. As discussed earlier in this section, the offset in the real self-energy is unknown a priori.

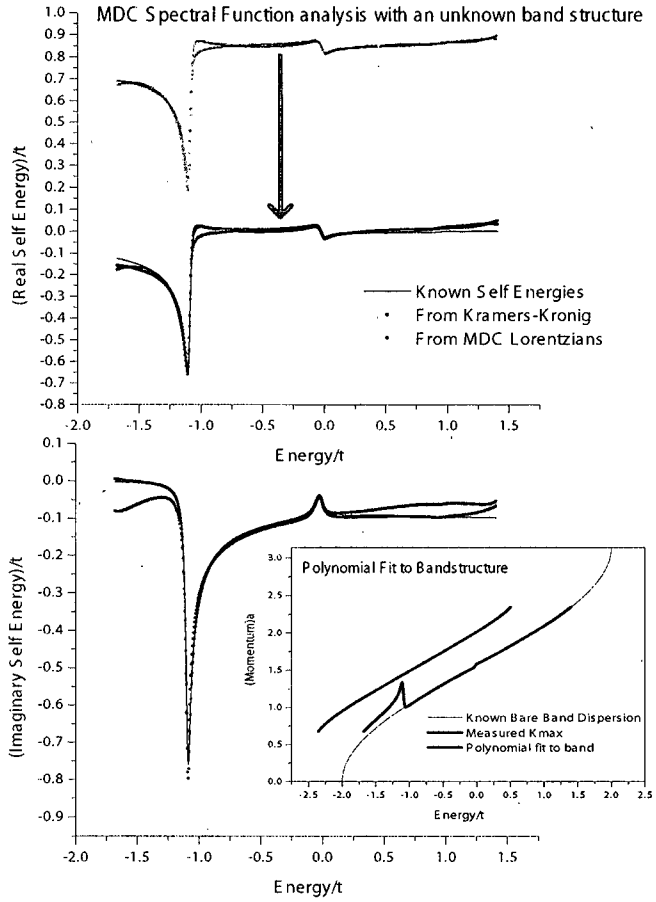

Figure 3.5: MDC Spectral Function analysis without a priori knowledge of the bare electron structure. Here a 6th order polynomial was used to fit the bare band, the parameters of which were adjusted until the Real and Imaginary parts of the self-energy, calculated using that polynomial band, are as self-consistent as possible. This self-consistency is measured through taking the Kramers-Kronig transform (with tails as described in § 3.1.4). As described under the limitations of this method, the bare band and real self-energy are only constrained to within an arbitrary energy constant. However, when shifted back into place the fit is good. $\Omega = 1.0$, $\lambda = 0.1$.

In reality this does not pose an insurmountable problem, if one has enough data to make use of the fact that the the real self-energy must go to zero at infinity. As can be seen in Figure 3.5 the procedure yields excellent results.

In previous studies other authors have had success by using either a linear [15] or quadratic [17] approximation to the bare electronic structure. While I found that it was sometimes possible to get reasonable results from a first or second order polynomial, it does not work in general. Figure 3.6 is a typical demonstration of the method of failure. Especially for small coupling, when the overall magnitude of the real self-energy is small, the real self-energy depends strongly on the distance between the bare band and the fit contour of MDC maxima. If the polynomial fit does not have sufficient freedom to follow the contours of the real band dispersion it will force the real self-energy to have un-physical behaviours.

As a final note - in these tests the curve fitting technique used simply follows the gradient to find a minima in χ^2, it makes no attempt to find *the* minimum. A global optimization routine was not used. Although usually the results found where good, occasionally the fitting routine would settle on something which is clearly not optimized. Since the *actual* band structure in known this did not pose a problem and these spurious results could be easily discarded. Usually, in these cases, the band structure was so far from realistic that it would be obvious even without a known band structure for comparison. However, when proceeding to study data in a case where the original band structure is unknown a global optimization scheme should be considered.

3.1.6 Resolution effects

In an actual experiment one can only hope to measure the spectral function to within the resolution of the analyzer used. With this in mind, a natural question would be what affect a finite instrumental resolution would have on the above procedure. In order to test resolution effects a 2D Gaussian convolution was performed on the data, with the FWHM across energy and momentum varied independently.

As one might expect, when the resolutions are significantly smaller than the widths of the features being measures there is little affect and the procedure described above yields reasonable results see Figure 3.7.

As the resolution gets larger, to approximately the same order of magnitude as the features to be measured, the effects can definitely be observed in the fitting procedure. To some extent the procedure can be improved by instead fitting a Voigt curve where the Gaussian component is known to be the

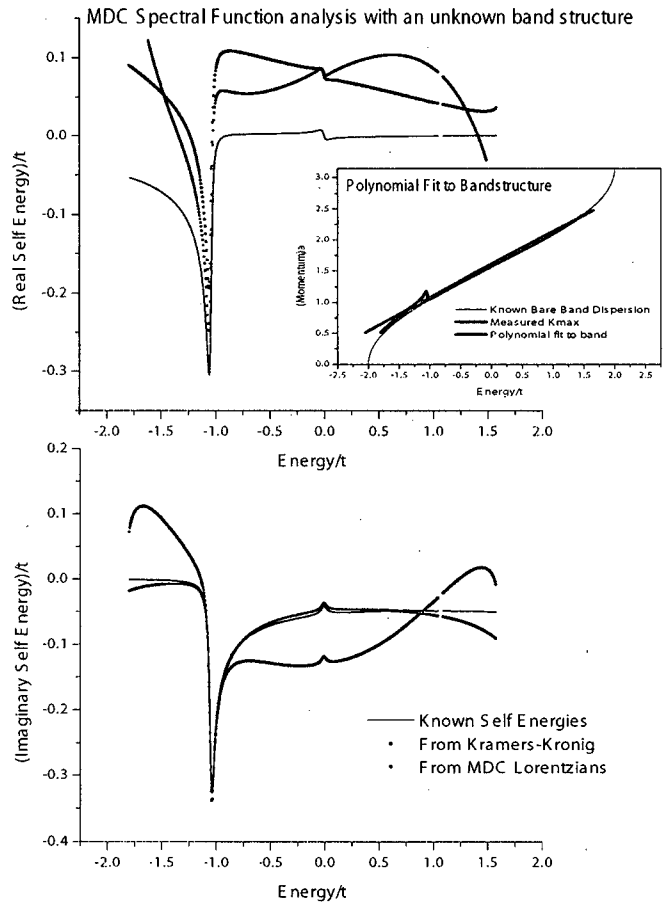

Figure 3.6: MDC Spectral Function analysis without a priori knowledge of the bare electron structure, where the polynomial fit is not of sufficient degree. Here a 2nd order polynomial was substituted for the bare band, however it does not have a sufficient order to follow the contours of the true underlying electronic structure. For this reason the real part of the self-energy can not be determined correctly, and the system is bound to failure. As can be seen, the self-energy arrived at has some qualitative behaviours similar to the true form, but the overall fit is poor and not self-consistent within the Kramers-Kronig transforms. $\Omega = 1.0$, $\lambda = 0.05$.

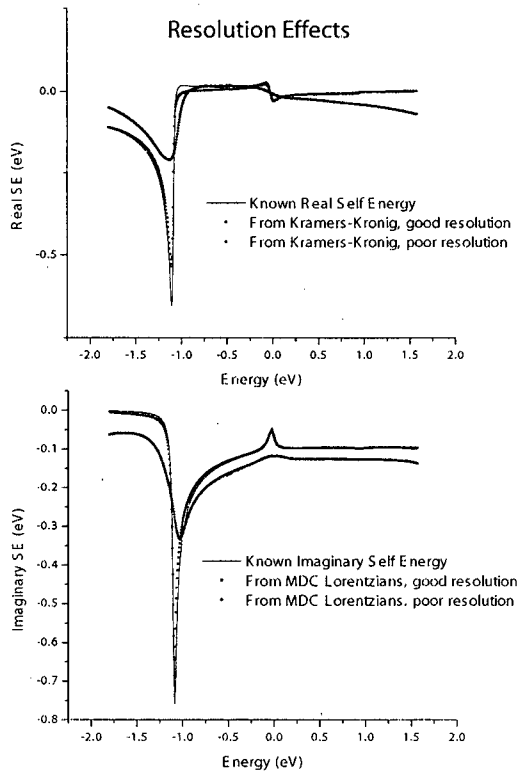

Figure 3.7: In order to study resolution effects on the self-consistent method of MDC spectral function analysis described here, a 2d convolution was done before attempting the same mechanism. Tests done at 'good' resolution were quite successful. This was modeled as a Gaussian broadening of FWHM 0.020 in the dimensionless energy and momentum units used. This would correspond to a resolution of 20meV and 0.02 inverse Angstroms for lattice spacing of 1 Angstrom and hopping energy 1eV - resolutions within the capacity of today's ARPES systems. Since most lattice spacings are greater than 1 Angstrom and typical hopping energies are smaller than 1eV this puts most system within this range. Tests were also done at 'poor' resolution one order of magnitude larger. While still qualitatively similar, the results were not promising for poor resolution systems. $\Omega = 1.0$, $\lambda = 0.1$.

instrumental resolution. This fixes the applied momentum broadening along only one dimension, however can not fix the effective momentum broadening caused by mixing from different energies and momenta. Since this broadening is both Gaussian in nature and drawn on from a range of energy and momenta it does *not* simply add in a ratio given by the band velocity as described in § 3.1.2 for Lorentzian broadening in the energy direction only.

3.1.7 Conclusions on MDC analysis

Through the MDC analysis described here one can measure the real and imaginary parts of the self-energy.

For this procedure, one can think of the bare band dispersion as a probe with which to measure the system. If the probe is well known, as in § 3.1.2 then the results can be quite successful and reasonably straightforward to obtain. However, as seen in § 3.1.5, often even in cases where the probe is unknown, it is still possible to extract the desired measurement - but one must study carefully both the probe and measurement together, checking for self-consistency. Through careful analysis of the spectral function alone one can discover both the bare electronic structure as well as the real and imaginary self-energy.

The most important limit on this procedure is that the self-energy be *momentum independent.* A necessary experiment, not performed in this thesis, would be to use a model with a momentum dependent self-energy and test whether or not incorrect, yet still self-consistent, results are possible with the procedure described here.

Other limits on this technique are to be expected. One must have data throughout the desired range, and at a resolution which is small compared to the features to be studied.

Overall, this method seems to be a promising addition to the ARPES technique.

3.2 Renormalization and EDC analysis

As noted above, in certain situations, it is possible to extract the full self-energy. But the self-energy is a rich function - what if the full self-energy is not required? And if the experimental window is too small, knowledge of the full self-energy within that window is of dubious utility. Additionally, the situations where the self-energy is available are limited - naturally one would like to be able to extract some meaning outside this small window. In these instances a simpler parameter would be more suitable.

In this section we will examine how from the /emphrenormalization of two simple parameters, *band velocity* and *bandwidth*, one can observe, qualitatively, the polaron behaviours discussed in Chapter 2.

3.2.1 Renormalization

Renormalization is a statement about how a given property scales due to the changing character of the quasi-particle as coupling is increased. As an illustrative example, we first examine how the observed *effective mass* might scale with increased coupling in a quasi-particle semi-conductor system.

Close to a maximum or minimum in the bare band dispersion, $\epsilon(k_0)$, it is often convenient to expand $\epsilon(k)$ in a Taylor series:

$$\epsilon(k) = \epsilon(k_0) + \epsilon'(k_0)(k - k_0) + \frac{\epsilon''(k_0)}{2}(k - k_0)^2 + \ldots \tag{3.11}$$

As k_0 is a max/min the linear term drops out, leaving us free to re-write the band dispersion in the neighborhood of k_0 as:

$$\begin{aligned} \epsilon(k) &\approx \frac{\hbar^2}{2m^*}(k - k_0)^2 \\ m^* &\equiv \frac{\hbar^2}{\epsilon''(k_0)} \end{aligned} \tag{3.12}$$

Where m^* is the *effective mass*. If expanded around a minimum we find that, for the purposes of semi-classical motion in electric and magnetic fields, the equations of motion behave as if describing a negatively charged particle of mass m^*. Similarly, if the expansion is around a maximum we find that they describe a positively charged particle of mass m^* (see, for example, Ashcroft and Mermin [1]).

When interactions are turned on the situation changes. The most major change is that there is no longer strictly even a *band*, as instead of a 1:1 relationship between energy and momentum we now have a probability distribution spread out over energy and momentum space[9]. However, the

[9]One might be tempted to call this probability density the *spectral function*, but this is not quite precise. Technically the spectral function (either A^+ or A^-) is either the one-particle addition or one-particle removal probability. Of course, one should immediately ask the question of what is actually important. It is not possible to measure, interact with, or observe properties which do not depend on the addition or removal of a particle from the ground state. This means, that while not strictly the distribution of electrons in the system, the *spectral function* is essentially the *observable* distribution, and (most importantly) the quantity we should be interested in.

concept of band still has utility. With this in mind we examine the *expectation value*, of energy as a function of momentum. Here the expectation value of energy at a given momentum is defined, in the usual way, from the Energy Distribution Curve (EDC) at that momentum:

$$\langle \epsilon \rangle (k) = \int_{\infty}^{\infty} \omega \cdot \mathrm{EDC}_k(\omega) \partial\omega \cdot \left(\int_{\infty}^{\infty} \mathrm{EDC}_k(\omega) \partial\omega \right) \tag{3.13}$$

We will likely find that the expectation value for energy, $\langle \epsilon \rangle (k)$, has a maximum or minimum allowing an expansion similar to Equation 3.2.1:

$$\begin{aligned} \langle \epsilon \rangle (k) &= \frac{\hbar^2}{2m^\dagger}(k - k_0)^2 \\ m^\dagger &\equiv \frac{\hbar^2}{\langle \epsilon \rangle'' (k_0)} \end{aligned} \tag{3.14}$$

Thus, due to interactions, an *effective mass renormalization* of $\frac{m^\dagger}{m^*}$ is observed. Quasi-particle renormalization is a widely used concept, which is often comparable between experiments. Its utility stems from the fact that it is often easily measured and still has physical meaning.

In practice, the effective mass concept can often be extended beyond just local maximum and minimum. The *band mass* refers to the local second derivative of the bare band structure (usually calculated from LDA) and is, in general, a function of momentum. When an experimentalist discusses *mass renormalization* it is most often a comment on the *band mass* defined in this way, as seen in Figure 3.8 and written:

$$\text{Band Mass Renormalization}(k) = \frac{\epsilon''(k)}{\langle \epsilon \rangle'' (k)} \tag{3.15}$$

In these cases the quasi-particle spectral weight must be distinguished from the spectral weight on the continuum. In practice this is often accomplished by either evaluating the integral in Equation 3.13 over a limited range, taking the expectation value to be the highest point in the EDC, or fitting the EDC with a functional form where the expectation value is know.

When comparing between experiments one must always be careful, as *renormalization* may mean different things. It may be due to the renormalized quantity being defined differently, or may simply be the ratio of some measured effective mass to electron rest mass. For example, the *mass renormalization* measured by de Haas-van Alphen (dHvA) measurements should, in principle, be the same as the band mass renormalization described by

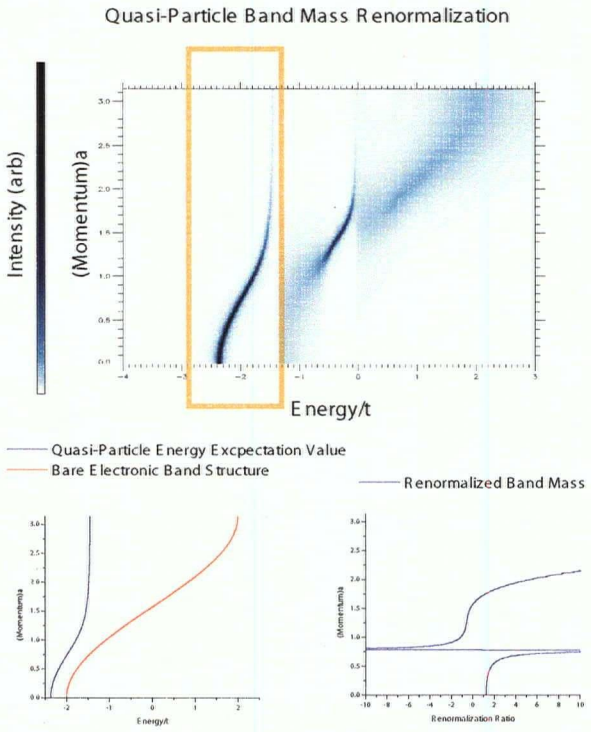

Figure 3.8: Band Mass Renormalization is taken as the ratio of second derivatives of the bare electronic structure and energy expectation value, Equation 3.15. Here we see the entire spectral function in the upper panel, with the quasi-particle highlighted. In the lower left panel we see both the energy expectation values, found via Equation 3.13, and the (known) bare band dispersion. In the lower right panel we see the renormalized band mass, which is a function of momentum. The coupling strength is $\lambda = 0.4$ and phonon energy $\Omega = 1.0$.

Equation 3.15[10] in going from a bare band to an interacting picture. However, what is commonly reported in dHvA measurements is the measured cyclotron mass expressed in terms of the electron mass[19], and not in terms of the cyclotron mass expected from the bare electronic band which is not calculated. Since ARPES typically measures a band mass renormalization these measurements should not be compared directly.

3.2.2 Quasi-particle band mass renormalization

Here we look at the band mass renormalization of our Holstein polaron problem as coupling is increased. As described above, we should direct our attention to energy expectation values, as a function of momentum. For this reason we take intensity of the spectral function as a function of energy for constant momentum, the EDC.

In this particular case, the expectation value of energy for the quasi-particle can be found easily by fitting each EDC curve with a Lorentzian, but depending on the system a more elaborate procedure might be required. The expectation value for each slice is then the Lorentzian center. The second derivative of these expectation values can be found numerically, and the band mass renormalization found with Equation 3.15. See Figure 3.8.

An examination of the second derivatives finds that the renormalization is constant in a momentum window around $k = 0$, before increasing sharply towards a discontinuity at the same momentum as the sharp kink in the quasi-particle dispersion. This is the manifestation of more phonon character at high momenta, as discussed in § 2.1.3.

Following this constant renormalization close to $k = 0$ in Figure 3.9, we see that the mass renormalization increases with coupling. This is also consistent with what we would expect based on the discussion in § 2.1.3.

We notice also that the function is monotonic, which means that provided we knew which curve to use (determined by the phonon energy, Ω), we could use this relationship to retrieve the coupling parameter λ from a measurement of band mass renormalization.

3.2.3 Bandwidth renormalization

Another quantity of interest is the quasi-particle bandwidth. As discussed in § 2.1.3 we should expect that the bandwidth occupied by the quasi-particle dispersion should decrease with increasing coupling. In the low

[10]For systems where mass renormalization is isotropic in the plane perpendicular to the magnetic field. See, for example, [1].

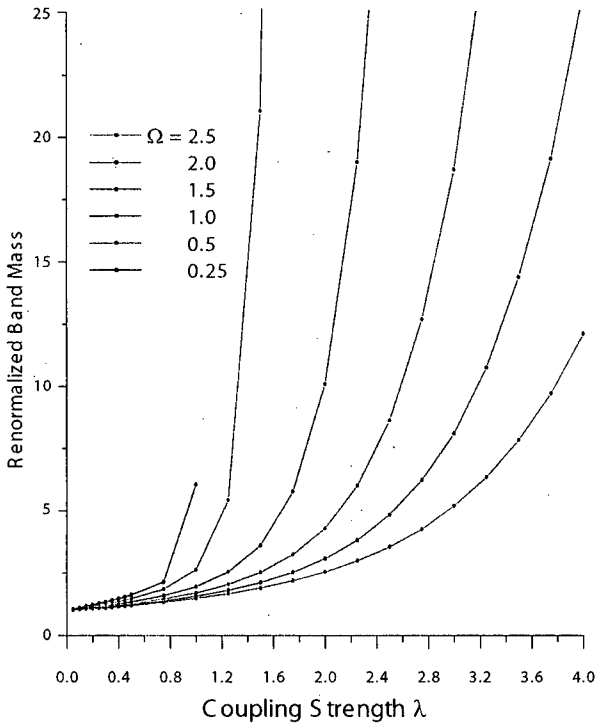

Figure 3.9: Band Mass Renormalization as a function of coupling strength λ and phonon energy Ω. We see that band mass renormalization is a sharply increasing function of coupling. This means that as coupling is increased the polaron quasi-particle is getting heavier due to the inclusion of more phonons.

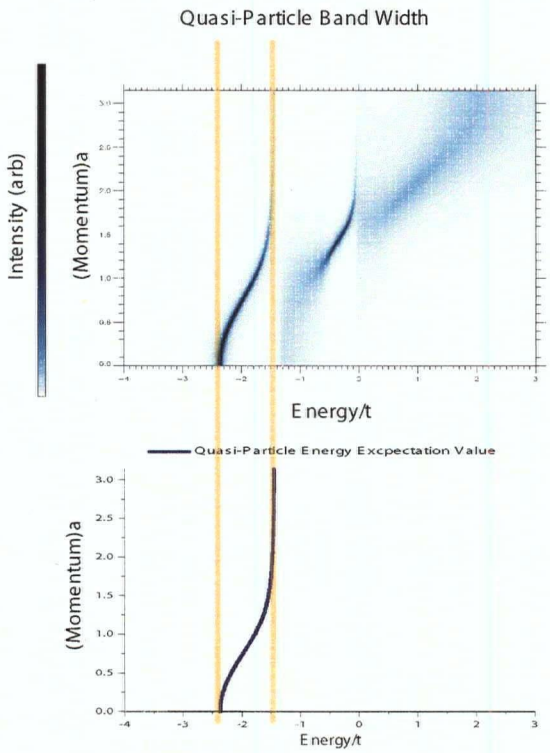

Figure 3.10: Quasi-particle band width is taken to be the distance between energy expectation values at $k = 0$ and $k = \pi$, highlighted in this figure.

coupling regime, immediately after splitting away from the continuum, it should have a bandwidth equal to the phonon energy, Ω. As coupling is increased and the polaron eventually becomes essentially frozen in the lattice at the high coupling limit the dispersion must evolve into the expected momentum delocalization. Therefore, we expect the bandwidth to go to zero at high coupling.

To define the bandwidth, EDC slices were again fit with a Lorentzian in the quasi-particle regime. The bandwidth was then taken as the distance between the maxima energy values at $k = 0$ and $k = \pi$. See Figure 3.10.

Following the measured bandwidth in Figure 3.11 as a function of coupling we see that it behaves as expected: At low coupling, the quasi-particle bandwidth is equal to the phonon energy. As coupling is initially increased the bandwidth is unaffected, as seen by the near zero slope near $\lambda = 1$ in the figure. Eventually, however, the bandwidth does asymptotically approach zero.

3.2.4 Coupling and phonon energy

As both band mass and band width were found to be monotonic functions of the coupling strength, one could imagine using the relationships found in Figures 3.9 and 3.11 to find the coupling strength, if phonon energy was known.

Ideally, one would be able to use the measurement of both bandwidth and mass renormalization in order to find both the phonon energy and coupling strength. As seen in Figure 3.11, in the extreme low-coupling limit the bandwidth is the phonon energy, making this determination possible.

Outside of this region, however, we find the relationships non-unique, and that a measurement of both quasi-particle bandwidth and mass renormalization only relates the two quantities. Thus, for most of the phonon energy-coupling parameter space, only qualitative properties of the phonons can be observed.

3.3 Conclusions

3.3.1 Self-consistent MDC spectral function analysis

In overview, the method described in § 3.1 can extract both the underlying bare electronic dispersion and the complex self-energy from a spectral function, with no a priori knowledge of the dispersion.

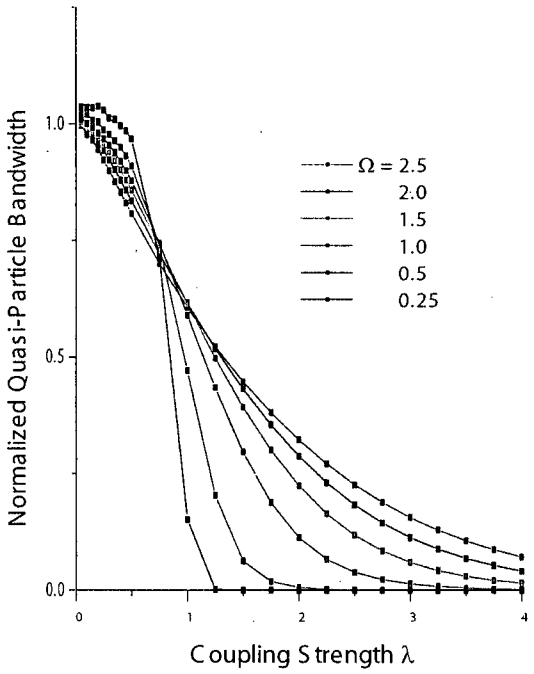

Figure 3.11: Band Width Renormalization as a function of coupling strength λ and phonon energy Ω. Here we see that slope is zero around $\lambda = 1$, indicating that in the low coupling limit the bandwidth does not immediately decrease with increasing coupling. Eventually, as expected, the bandwith will asymptotically go to zero.

Procedure

Once the spectral function has been collected over some range the first step is to do a Lorentzian peak fit for every MDC. This generates the peak position k_m and HWHM from each fit as a function of energy.

Next, some functional form for the bare band electronic dispersion must be chosen. It need not be physically meaningful, but it must be able to reasonably approximate the bare band dispersion over the range of peak position momenta, k_m, collected.

From this test bare band dispersion Equation 3.7 is used to generate a complex self-energy. In general, this first self-energy generated will not be correct as it was not based on the correct bare band dispersion. This calculated self-energy is checked for self-consistency via the Kramers-Kronig relationships (Equation 3.10).

An iterative fitting procedure must then be used, where the parameters of the bare band model are varied using self-consistency as measured via the Kramers-Kronig relationships as the guide. Once the Kramers-Kronig relationships are self-consistent one has confidence that the guessed bare band dispersion is correct, to within a constant energy offset. This constant offset affects both the bare band dispersion and the real part of the self-energy as discussed in § 3.1.5.

Since the real part of the self-energy must go to zero at infinity, this constant offset can simply be shifted once the parameters of best fit have been found.

Thus, this method can be used to measure the real and imaginary parts of the self-energy as well as the bare band dispersion from the spectral function.

Limitations

Some of the limitations to this technique are to be expected. One must have data throughout the desired range, and at a resolution which is small compared to the features to be studied. The most important limitation on this procedure is that the self-energy be *momentum independent.*

Conclusions

A necessary experiment, not performed in this thesis, would be to use a model with a momentum dependent self-energy to discover what consequences this effects.

Although this final caveat should still be examined, this method appears to be a promising addition to the ARPES technique as with no a priori knowledge of the dispersion it can extract both the underlying bare electronic structure and the complex self-energy.

Of course, now that the results have been verified by a model with realistic form, the true test will be to apply this technique to actual ARPES data.

3.3.2 Qualitative EDC analysis

As seen in § 3.2, even when a quantitative determination of the self-energy from the spectral function is not possible, or simply not desired, a qualitative study of data is still possible through the study of quasi-particle mass renormalization and quasi-particle bandwidth renormalization.

We saw in the Holstein polaron model, that as we turn on coupling the bare band splits into a quasi-particle peak and continuum. The character of this quasi-particle changes with both momentum and coupling strength. As coupling increases the quasi-particle will have a larger phonon cloud due to the stronger interactions. Also, a sharp flattening in the quasi-particle dispersion relation was observed, indicating that a larger phonon cloud was also present at high quasi-particle momenta.

As coupling is increased further, we saw that the quasi-particle takes on a progressively larger phonon cloud, increasing its weight and narrowing its bandwidth. This continues until the quasi-particle bandwidth narrows to zero in the high-coupling limit.

Through the examination of the band mass renormalization and the bandwidth renormalization one has access, qualitatively, to the rich polaron behaviours as discussed in Chapter 2.

Bibliography

[1] Ashcroft and Mermin. *Solid State Physics.* Thomson Learning, first edition, 1976.

[2] Mona Berciu. Green's function of a dressed particle. *Physical Review Letters*, 97(3):036402, 2006.

[3] Mona Berciu and Glen L. Goodvin. Systematic improvement of the momentum average approximation for the green's function of a holstein polaron. *Physical Review B (Condensed Matter and Materials Physics)*, 76(16):165109, 2007.

[4] A. Damascelli. *Physica Scripta*, T109:61–74, 2004.

[5] Philippe Dennery and André Krzywicki. *Mathematics for Physicists.* Dover, first edition, 1967.

[6] P. A. M. Dirac. The quantum theory of the emission and absorption of radiation. *Proceedings of the Royal Society of London. Series A, Containing Papers of a Mathematical and Physical Character*, 114(767):243–265, mar 1927.

[7] A. Einstein. *Ann. Phys.*, 31:132, 1905.

[8] Glen L. Goodvin, Mona Berciu, and George A. Sawatzky. *Phys. Rev. B*, 74:245104, 2006.

[9] Lars Hedin, John Michiels, and John Inglesfield. Transition from the adiabatic to the sudden limit in core-electron photoemission. *Phys. Rev. B*, 58(23):15565–15582, Dec 1998.

[10] H. Hertz. *Ann. Phys.*, 17:983, 1887.

[11] T. Holstein.

[12] S. Hüfner. *Photoelectron Spectroscopy: Principles and Applications.* Springer, 2003.

[13] N. J. C. Ingle, K. M. Shen, F. Baumberger, W. Meevasana, D. H. Lu, Z.-X. Shen, A. Damascelli, S. Nakatsuji, Z. Q. Mao, Y. Maeno, T. Kimura, and Y. Tokura. Quantitative analysis of sr[sub 2]ruo[sub 4] angle-resolved photoemission spectra: Many-body interactions in a model fermi liquid. *Physical Review B (Condensed Matter and Materials Physics)*, 72(20):205114, 2005.

[14] D W Johnson. A fourier series method for numerical kramers-kronig analysis. *Journal of Physics A: Mathematical and General*, 8(4):490–495, 1975.

[15] Adam Kaminski and Helen M Fretwell. On the extraction of the self-energy from angle-resolved photoemission spectroscopy. *New Journal of Physics*, 7:98, 2005.

[16] Frederick W. King. Efficient numerical approach to the evaluation of kramers-kronig transforms. *J. Opt. Soc. Am. B*, 19(10):2427–2436, 2002.

[17] A. A. Kordyuk, S. V. Borisenko, A. Koitzsch, J. Fink, M. Knupfer, and H. Berger. Bare electron dispersion from experiment: Self-consistent self-energy analysis of photoemission data. *Physical Review B (Condensed Matter and Materials Physics)*, 71(21):214513, 2005.

[18] Löwen. *Phys. Rev. B*, 37:8661, 1988.

[19] A. P. Mackenzie, S. R. Julian, A. J. Diver, G. J. McMullan, M. P. Ray, G. G. Lonzarich, Y. Maeno, S. Nishizaki, and T. Fujita. Quantum oscillations in the layered perovskite superconductor sr_2ruo_4. *Phys. Rev. Lett.*, 76(20):3786–3789, May 1996.

[20] Alexandru Macridin. *Phonons, charge and spin in correlated systems.* PhD thesis, Rijksuniversiteit Groningen, 2003.

[21] Richard D. Mattuck. *A Guide to Feynman Diagrams in the Many-Body Problem.* Dover, 1976.

[22] John P. Perdew and Yue Wang. Accurate and simple analytic representation of the electron-gas correlation energy. *Phys. Rev. B*, 45(23):13244–13249, Jun 1992.

[23] M.P. Seah and W.A. Dench. *Surf. Interface Anal.*, 1:2, 1979.